Monitoring of the recovery of ion-damaged 4H-SiC with in-situ synchrotron X-ray diffraction as a tool for strain-engineering

Anusmita Chakravorty, Alexandre Boulle, Aurélien Debelle, Isabelle Monnet, Gouranga Manna, Pinku Saha, Mrinmay Kumar Mukhopadhyay, Debdulal Kabiraj

Monitoring of the recovery of ion-damaged 4H-SiC with in-situ synchrotron X-ray diffraction as a tool for strain-engineering

Anusmita Chakravorty[1], Alexandre Boulle[2], Aurélien Debelle[3], Isabelle Monnet[4], Gouranga Manna[5], Pinku Saha[6], Mrinmay Kumar Mukhopadhyay[7] and Debdulal Kabiraj[1*]

[1*]Inter-University Accelerator Centre, Aruna Asaf Ali Marg, New Delhi 110067, India.
[2]Institut de Recherche sur les Céramiques (IRCER), CNRS UMR 7315, 12 rue Atlantis, Cedex, Limoges 87068, France.
[3] IJCLab, Université Paris-Saclay, CNRS/IN2P3, Institut de Physique des 2 Infinis Irène Joliot-Curie, Orsay 91405, France.
[4] Normandie Univ, ENSICAEN, UNICAEN, CEA, CNRS, Centre de recherche sur les Ions, les matériaux et la photonique, 14000 Caen, France.
[5]Chemistry and Physics of Materials Unit, Jawaharlal Nehru Centre for Advanced Scientific Research, Rachenahalli Lake Rd, Jakkur, Bengaluru, Karnataka 560064, India.
[6]National Centre for High Pressure Studies, Department of Physical Sciences, Indian Institute of Science Education and Research Kolkata, Mohanpur Campus, Mohanpur, 741246 Nadia, West Bengal, India.
[7]Surface Physics and Material Science Division, Saha Institute of Nuclear Physics, 1/AF Bidhannagar, Kolkata 700064, India.

*Corresponding author(s). E-mail(s): kabiraj@iuac.res.in;
Contributing authors: anusmitachakravorty@iuac.res.in;

Abstract

In-situ thermal annealing (673-1273 K) during X-ray diffraction synchrotron measurements was performed to monitor the strain level as a proxy to follow the recovery of 300 keV Ar ion irradiated 4H-SiC single crystals. Results show that, when exposed to Ar ions at a fluence of 6.7×10^{14} ions/cm^2 (0.7 dpa), the material suffers a maximum strain of 12% that reduces to 2% after the final anneal at 1273 K. In the same time, the disorder derived from the XRD data also demonstrates a thermal recovery of the crystalline structure. Hence, this work presents ion irradiation as a means to induce specific crystalline order and depth-controlled strain states within a few 100s of nm window in 4H-SiC.

Keywords: 4H-SiC, Ion-irradiation, lattice damage, Strain-engineering, Synchrotron single-crystal XRD, Thermal recovery

1 Introduction

Silicon carbide is a well-established industrial semiconductor material [1–4]. The modern-day technology involves ion beam irradiation as a tool to tune the device-worthy characteristics of SiC [5]. This calls for an extensive research to engineer its material properties desired for opto- and micro-electronics applications. For example, the defects in the material that are introduced during application or fabrication might cause adverse effects on the optoelectronic properties. The structural distortions of the crystalline lattice in the vicinity of defects also lead to a mechanical strain. Likewise, the structural effects such as strain engineering using ion beams can be viewed as an effective way to recover the desired properties since the strain results in shifting of the defect levels and band edges. Effective utilization of this energy level-shifting can eliminate the undesired defect states within the bandgap. Several studies have experimentally and theoretically determined that significant lattice strain is induced in SiC after various ion irradiation [6–8]. Recently, it has been demonstrated that strain relaxation occurs from ionization-induced annealing of 21 MeV Ni ion in predamaged 4H-SiC [9]. Also, we recently verified that the rapid thermal-spike caused by the strong ionizing energy deposited by 100 MeV Ag ions results in structural and chemical damage recovery in 4H-SiC [10]. Besides, the role of swift heavy ion irradiation in the generation of controlled defects has also been studied [11]. Further, we have also investigated thermal and ion beam-induced ultrafast thermal spike-assisted annealing of pre-damaged 4H-SiC with initial damage as 0.3 dpa (dpa; displacement per atom, 1 dpa = all atoms are displaced at least once from their respective lattice sites) [12, 13]. This damage level marks the saturation of the first step of damage build-up where the lattice has isolated point defects and a smaller number of in-cascade clusters (ref.[12] and references therein). The present work has a two-fold objective: (i) to advance understanding of ion irradiation effects and (ii) utilize those for

strain-engineering in 4H-SiC. Furthermore, because strain engineering is a current topic of research interest [14] in semiconductor materials, the monitoring of strain before and after thermal treatment, is given considerable emphasis.

In this experimental work, we have irradiated <0001> 4H-SiC single crystals to create specific disordered states using ion irradiation. In the case of low energy ions, having few 100s of keV energy, the energy loss is dominated by the elastic collision (also referred to as ballistic) process that leads to atomic displacements. The slowing down of energetic ions produces defects by binary collision through Coulomb interaction between the screened nuclear charge of projectile and target nuclei. Radiation-induced modifications, such as crystalline to an amorphous phase transition, in SiC due to energy deposited to atomic nuclei via scattering collisions have been the subject of various experimental efforts [15–19]. The current study investigates the modifications in the crystalline order resulting from irradiation with Ar ions in the ballistic regime followed by thermal treatment using principally high-resolution X-ray diffraction (HR-XRD) to monitor the strain and disorder levels, complemented by Channeling-Rutherford backscattering spectrometry (RBS/C), Raman spectroscopy and transmission electron microscopy (TEM). In-situ synchrotron thermal treatment allowed annealing the same ion-damaged sample to different temperatures and performing HR-XRD measurements. This prevented any difference in signal that might have occurred between two samples having the same experimental history. Besides, synchrotron-based measurements enabled the detection of large-scale variations in the diffraction signals.

2 Experimental

The n-type 4H-SiC <0001> single-crystal wafer used for the experiment were procured from Semiconductor Wafer Inc. The wafer was chopped into pieces with dimensions of $\sim 1 \times 1$ cm^2. The low energy ion irradiations using 300 keV Ar were performed at room temperature (RT) using the Low Energy Ion Beam Facility at the Inter-University Accelerator Centre (IUAC) in New Delhi, India. To reduce the channeling effect, irradiation was done at a 7° tilt angle, and to avoid sample heating, the beam current was set to 100 pnA (particle nanoampere; 1pnA $= 6.25 \times 10^9$ ions/s) during irradiation. Before performing ion-irradiation, TRIM full-cascades simulations [21, 22] were run to extract the damage with depth profiles in terms of dpa. For TRIM simulations, the threshold displacement energies of 20 and 35 eV were used for the C and Si, respectively [23]. The Ar fluences used in the present experiment along with their TRIM estimated maximum dpa values are: (i) 9.6×10^{13} ions/cm^2 (0.1 dpa) (ii) 6.7×10^{14} ions/cm^2 (0.7 dpa) and (iii) 9.6×10^{14} ions/cm^2 (1 dpa). Hereafter the samples will be referred to by their corresponding dpa values. The Pelletron Accelerator RBS-AMS Systems facility at IUAC was used to perform RBS/C measurements with 2 MeV He^+ ions and a detector located at an angle of 166°. The Raman spectra were acquired at RT using the WITec GmbH Raman spectrometer with a green laser light of 532 nm at AIRF, JNU,

India. Transmission electron microscopy (TEM) characterizations were carried out on three selected samples using a microscope operated at 200 keV (JEOL F200). For this purpose, X-sections were prepared (at CIMAP in Caen, France) using the focused-ion-beam method with a Helios Nanolab 660 equipped with Ga^+ ions accelerated at 30 keV (decreased down to 2 keV for the final steps). Bright-field images were recorded. HR-XRD was performed using the 18B KEK beamline of the Photon Factory synchrotron facility in Japan. Because of the monochromatic high flux and improved collimation, synchrotron-based in situ X-ray diffraction has higher sensitivity and resolution over the traditional lab-based XRD. This enables the detection of otherwise undetected features, as demonstrated hereafter. Single-crystal rocking curve measurements were carried out for sample alignment followed by symmetrical high-resolution θ-2θ scans around the (004) reflection using a wavelength of $1.2384\mathring{A}$ and the data were recorded with a scanning step of 0.001° (see Supplementary for details). To study recovery effects, the crystal with a disorder level of 0.7 dpa, characterized by the presence of an extended amorphous/heavily-damaged region, was chosen as the reference sample to monitor the effect of the thermal treatments. In-situ thermal annealing was performed on the sample inside the beamline at temperatures ranging from 673 to 1273 K with a 10 K/min ramp. The sample was kept at each temperature step for 30 minutes and then cooled to ambient temperature, followed by HR-XRD measurements. The strain (i.e. the relative lattice parameter change) and disorder (namely the static Debye-Waller factor) depth-profiles were retrieved by simulation of the XRD patterns using the RaDMaX-online program specifically developed for that purpose [24, 25]. For the simulation, RaDMaX implements the recursive solution to the Takagi-Taupin equations [26, 27] which describes dynamical diffraction from distorted crystals [28].

3 Results and discussion

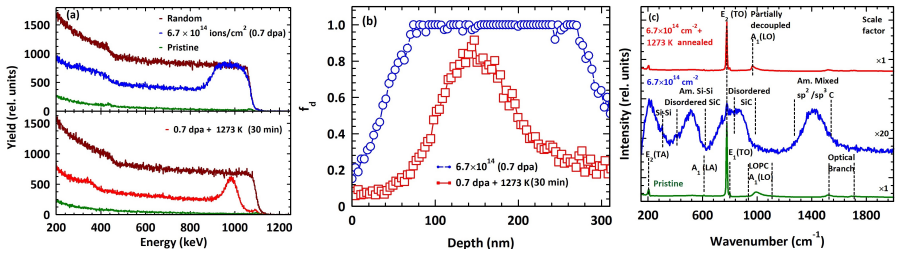

Fig. 1 (a) RBS/C spectra recorded on 4H-SiC after 300 keV Ar irradiation with fluence of 6.7×10^{14} ions/cm^2 , and after subsequent thermal annealing of the sample at 1273 K for 30 mins and (b) is the corresponding depth profiles of disorder (f_d) extracted using DICADA.[20] (c) Raman spectra of the pristine, irradiated and annealed sample.

As shown in Figure 1(a), the RBS/C yield of the 0.7 dpa sample reaches the random level, indicating that the lattice has entered amorphization. From

the corresponding damage with depth profiles (Figure 1(b)), it is clear that the amorphous region, where the RBS/C yield reaches the random level, has a width of ∼200 nm with centre at ∼175 nm. The effect of thermal annealing appears as a reduced width of the amorphous region, and a decreased overall RBS/C yield, suggesting recovery of the ion-induced lattice damage. The extent of recovery is found to depend on the amount of surrounding crystalline regions around the amorphous/disordered regions, as evident from the higher recovery observed at the boundaries of the crystalline-amorphous region as compared to the centre. This is consistent with previous studies where it has been concluded that epitaxial recrystallization requires a sufficient amount of crystalline surroundings that acts as the deciding factor for the extent of observed damage recovery [10, 11, 29, 30]. Annealing at 1273 K for 30 min recovers significant damage, however, the RBS/C yield remains much greater than that of the pristine. To quantitatively assess damage annealing, recovery percentage [10, 11] is estimated to be 54.4%. The recovery percentage is evaluated using the data shown in Figure 1(b). For percentage calculations, the difference in the total disorder before (f_d^{before}) and after thermal annealing (f_d^{after}) is divided by f_d^{before}. The total disorder in the damaged sample, with respect to the pristine sample, is estimated over the entire pre-damaged depth by summing up the disorder evaluated using an ad hoc simulation code, named DICADA [20] to fit the RBS/C profiles. A significant disorder persists in the lattice that would need additional treatment for a more pronounced recovery [31].

A reduced backscattering yield in the RBS/C spectra can follow from a partial recovery of the crystal due to annealing of the pre-existing defects, and hence provides information on the long-range order, while Raman is more sensitive to the short-range arrangements of atoms. In the Raman spectra presented in Figure 1(c), the various first-order modes and other Raman active modes are identified based on previous reports [17, 32–39]. The Ar induced disorder in the crystal structure of 4H-SiC results in a drop in the strength of the first-order Raman peaks and the emergence of new bands that may be attributed to the homonuclear Si-Si (∼260cm^{-1}) and C-C (∼1400cm^{-1}) bonds. The bands related to disordered SiC are also observed between 400-600cm^{-1} and 800-1000 cm^{-1}. The Raman spectra (see Figure 1(c)) obtained after thermal annealing at 1273 K is identical to that of pristine 4H-SiC, and the bands linked to disordered SiC and homonuclear Si-Si/C-C bonds are considerably suppressed. The intensity of the dominating E_2 (TO) Raman mode at 778 cm^{-1} is dramatically increased and the A_1(LO) at around 980 cm^{-1} is partially decoupled from A_1 longitudinal optical phonon–plasmon coupled (LOPC) mode after annealing. Before and after thermal annealing, the calculated disorder values from Raman data are 0.39 and 0.18, respectively. The disorder from Raman is estimated as 1-A, where A is the sum of the area under the first-order Raman modes in the irradiated material normalized with respect to that of the pristine crystal [10, 11, 17]. The percentage of recovery calculated in this case is 52.1%. Annealing in the temperature range of 373-1073 K

is insufficient to allow notable recrystallization of completely amorphized layers formed by ion irradiation of 4H-SiC [40]. In the present experiment, the annealing is performed at a higher temperature (1273 K) and the recovery is significant but not complete, as viewed by RBS/C and Raman.

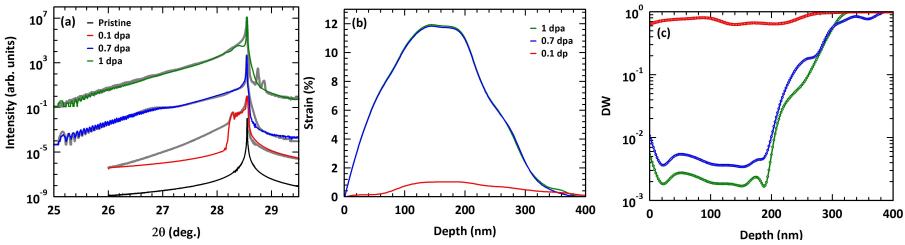

Fig. 2 (a) Evolution with increasing ion fluence of the 004 peak in HR-XRD profiles of 4H-SiC irradiated with fluences of 9.6×10^{13} ions/cm^2 (0.1 dpa) , 6.7×10^{14} ions/cm^2 (0.7 dpa) and 9.6×10^{14} ions/cm^2 (1 dpa) using 300 keV Ar ions. Colored lines are results of simulations and the grey lines represent the experimental data. (b) and (c) are the corresponding Strain and DW depth profiles obtained from the simulation of HR-XRD curves.

Based on TRIM simulations and RBS/C results, the damage in 4H-SiC after 300 keV Ar ion irradiation is within ∼300 nm thickness, with peak damage at a depth of about 175 nm [10, 13]. Following ion irradiation, the crystals were also examined using HR-XRD in θ-2θ mode to determine the variation of strain with depth. The HR-XRD profiles of pristine and Ar irradiated 4H-SiC are shown in Figure 2(a). In the pristine 4H-SiC crystal, the 2θ position of the (004) Bragg peak is observed at 28.55°. After 300 keV Ar ion irradiation, an additional signal appears at lower angles indicating the presence of a dilatation gradient in the direction normal to the surface. The peak from the undamaged zone remains visible because the damage depth for the 300 keV Ar ion irradiation in 4H-SiC (∼300-350 nm according to TRIM) is significantly less than the X-ray penetration depth ∼8.25 μm (for an incident angle of 14.2°; Bragg angle for 4H-SiC) for the X-ray energy we used (∼ 10keV). However, since the lattice parameter of both regions differs, the XRD signals can be easily separated. Not only can they be separated but also the complete XRD signal can be entirely fitted with an appropriate physical model. The oscillations that can be noticed in the HR-XRD pattern are related to interferences between the scattered X-rays emerging from the damaged regions of varying strain [41].

In Figure 2(a), in addition to the scattering from the strain profile described above, two other features can be noticed. At 0.1 dpa there is a strong diffuse scattering signal below $2\theta = 28.2°$. It most likely comes from surface contamination and was not included in the simulations. At 1 dpa, two additional peaks appear at higher values of 2θ between 28.8-29°, whose exact origin remains to be investigated. Yet, their intensity is more than 10^6 times weaker than the main signal and can therefore be easily neglected in the simulation procedure. Despite the presence of these unusual features it was possible to reliably

simulate the XRD signal emanating from the strain/disorder gradient over an intensity range of 10^8 which is, in general, a very challenging task.

These simulations are presented in Figure 2(a), with the associated strain (Figure 2(b)) and Debye-Waller factor (Figure 2(c)) depth profiles. The HR-XRD data obtained from synchrotron measurements allowed having very large intensity dynamics. This enabled discrimination between two apparently fully amorphous layers (0.7 and 1 dpa), as there exists a noticeable difference in the DW values in the sub-surface region (Figure 2(c)). It should be noted that with a laboratory based XRD setup, with a dynamic range of 10^4-10^5, differentiating between these two samples would have been impossible. Figure 2(a) depicts the simulated XRD curves as colored lines. The strain profiles are slightly asymmetric and extend to a depth of about 400 nm from the sample surface. These findings are in great agreement with the damage profiles predicted by TRIM and previously determined by RBS/C. The degree of strain grows as the fluence increases from 0.1 to 0.7 dpa, whereas the position of the strain maximum stays unchanged. Further increasing the fluence from 0.7 to 1 dpa, the strain profile is almost unchanged, indicating a saturation with 12% maximum strain. This observation reveals that after the formation of an extended amorphous region, further increasing the ion fluence, the strain in the damaged 4H-SiC layer reaches a saturation value. The strain level experienced by the irradiated layer (12%) is extremely high, but such a level has been reported already by S. Leclerc et al.[42]. Another parameter that is evaluated for simulation of the XRD profiles is the static Debye-Waller (DW) factor, which causes the diffracted amplitude to decrease [43]. The DW factor for a perfect single crystal 4H-SiC is 1 and the disorder fraction obtained from the HR-XRD simulations is defined as 1-DW [8]. Previous research on irradiation of SiC indicated that the DW factor may be immediately translated into the volume fraction of amorphized or severely disordered material for a particular reflection [6–8, 44]. As a result, the production of amorphous or severely disordered inclusions may be directly attributed to the decrease of the coherent intensity. From Figures 1(b) and 2(c), in the amorphous-like region between 20 to 200 nm, a resemblance can be observed in the variation of RBS/C disorder and 1-DW. Also, it must be pointed out that the parts of the irradiated layer that exhibit the high strain level is extremely small, as indicated by a very low DW factor (see Figures 2(b) and 2(c)) in the 12% strain region. A last result to point out is the difference between the 0.7 and 1 dpa irradiated crystals. Indeed, both exhibit an amorphous structure, as shown by RBS/C [11] but, as mentioned earlier, due to the high sensitivity of the synchrotron measurement, it is here possible to discriminate between the two, as a clear difference in the Debye-Wallor factor is readily observed in the 20-180 nm region (see Figure 2(c)).

The HR-XRD results after annealing of the 0.7 dpa sample at various temperatures in the range 673-1273 K are presented in Figure 3(a). The curve for 0.7 dpa shows oscillations near 25° and a hump at around 26.8°. With increasing annealing temperature, the strain-related oscillations start to shift towars

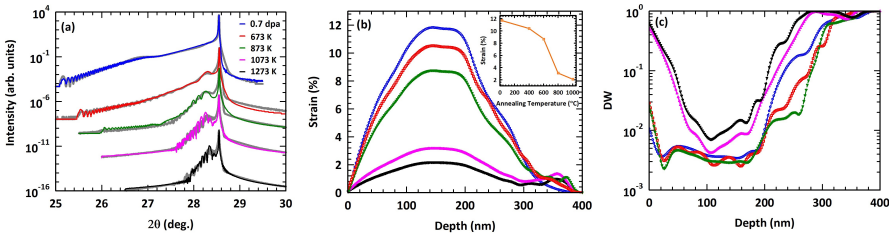

Fig. 3 (a) HR-XRD profiles of 4H-SiC irradiated with fluence of 6.7×10^{14} ions/cm^2 (0.7 dpa) using 300 keV Ar ions and annealed at various indicated temperatures. Colored lines are results of simulations and the grey lines represent the experimental data. (b) and (c) are the corresponding Strain and DW depth profiles. Inset to (b) shows the variation of strain(%) at 175nm with annealing temperatures. Connecting line is drawn to guide the eyes.

the main Bragg peak which is a signature of strain relaxation. This suggests that more lattice sites are recovering and attaining a similar lattice structure as the parent sample. The strain profiles, shown in Figure 3(b), are almost regular bell-shaped with a maximum strain at ∼175 nm that extends down to 400 nm from the sample surface. Annealing at 1073 K and 1273 K leads to a substantial reduction in the maximum strain from 12% to 3% and 2%, suggesting significant recovery of the lattice. This recovery agrees with the experimental results obtained from RBS/C and Raman analyses. The corresponding DW depth profiles are presented in Figure 3(c). For the first three anneals, the DW factors almost overlap except for depths beyond 200 nm. On increasing the annealing temperature to 1073 K and 1273 K, the DW factor (Figure 3(c)) evaluated over the entire pre-damaged depth (∼300 nm) shows movement towards recovery. Interestingly, as observed also by RBS/C, the recrystallization is initiated from the boundaries of the crystalline-amorphous region. The variation of strain at the peak damage depth of 175 nm with isochronal annealing is shown in the inset of Figure 3(b). Furthermore, as shown in Figure 4, the activation energy of the strain release, in the temperature range 873-1273 K, is estimated using the Arrhenius plot of strain-relaxation vs. inverse temperature. The activation energy is estimated to be 0.29 eV. The observed strain recovery can be explained based on activation and recombination of defects [45, 46].

Previously, it has been reported that the recovery in 4H-SiC is a three-stage process [45, 46]. The recovery mechanisms and the temperature ranges are: (i) Stage I: Frenkel pair (FP) recombination of C or Si at 250∼420 K, (ii) Stage II: migration of interstitials at 470∼570 K, and (iii) Stage III: migration of vacancies 600∼700 K. However, in our case, the obtained results show that thermal relaxation of strain exhibits a discontinuous behavior marked by two stages operating at different temperature regimes. The first stage lasts upto 873 K and the second annealing stage starts at a temperature above 873 K, showing a discontinuity in the reduction of strain. The first stage of strain relaxation can be linked to the FP recombinations and the second stage is possibly due to the additional migration and recombination of the self-interstitials as well as the vacancies. From a recent report [47], a proposed route for this annealing

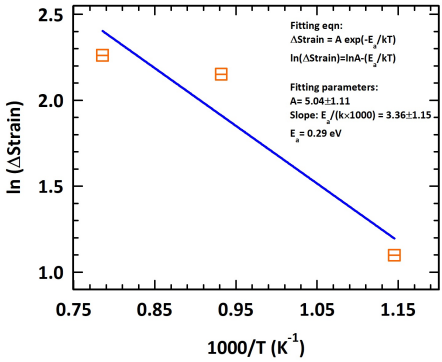

Fig. 4 Arrhenius plot of strain recovery for thermally annealed 0.7 dpa 4H-SiC. The change in strain(%) w.r.t pristine is calculated at 175nm using Figure 3(b). The blue connecting line is the line of best fit.

can be ascribed to the recombination of V_{Si} with migrating silicon interstitial I_{Si}. Photoluminescence-based thermal annealing studies of the V_{Si} defects in 4H-SiC also show that annealing at above ∼873 K decreases the luminescence signals, indicating a decrease in the V_{Si} defects.[48–50]

Finally, using Figure 1(b), an attempt is made to estimate the fraction of atoms recovered to release the lattice strain from 12% to 2%. From Figure 3(b), it can be seen the strain profile is almost flat within a window of 140-180 nm from the sample surface. Thus, in our estimation, we only consider the atoms that lie within this window. The calculation is as follows:

- No. of atoms within $1\mathrm{cm}^{-3}$ volume of 4H-SiC = 9.64×10^{22}
- No. of atoms within pre-damage (140 -180nm) = 3.9×10^{17}
- Fraction of atoms creating the disorder = 0.98
- Fraction of atoms creating the remaining disorder after annealing at 1273 K = 0.79
- Fraction of atoms replaced/recovered after 30min annealing at 1273 K = 0.19

In the above calculations, the values 0.98 (before annealing) and 0.79 (after annealing) are derived by considering the fraction of area under the DICADA profiles between 140-180nm (Figure 1(b)). Finally, the obtained values are subtracted to estimate the fraction of atoms recovered. Thus, it can be estimated that the reduction in strain from 12% to 2% (140-180 nm) resulted from the movement of about 19% of atoms ($\sim7\times10^{16}$) back to the required lattice sites in 4H-SiC. Using similar calculations, it can also be estimated that annealing at 1273 K allowed the movement of about 1.6×10^{18} atoms in the entire pre-damaged region (∼300 nm) back to the required lattice sites in 4H-SiC.

Finally, a transmission electron microscopy study was undertaken to acquire a clearer picture of the microstructure associated with the pre-damaged and annealed 4H-SiC crystals. The TEM images as well as their corresponding

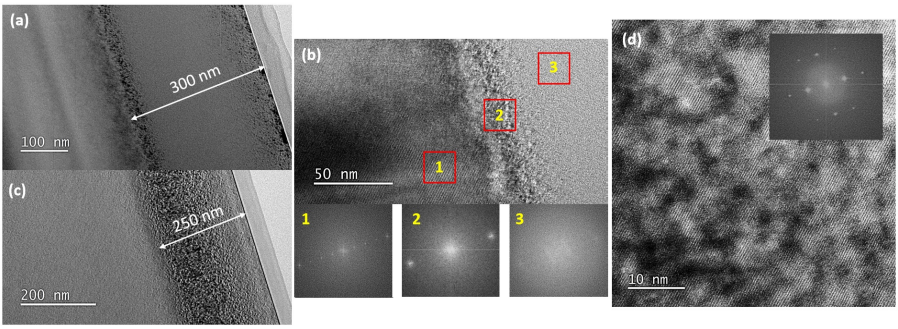

Fig. 5 Cross-sectional TEM images recorded with <0001> planes perpendicular to the surface for 4H-SiC crystals irradiated with 300 keV Ar ions at: (a),(b) 7.7×10^{14} ions/cm^2 (0.8 dpa) and (c),(d) 6.7×10^{14} ions/cm^2 (0.7 dpa) + annealed at 1273K for 30 mins. 1, 2 and 3 present the fast Fourier transforms (FFTs) of some selected regions indicated by squares in (b). Inset to (d) present the corresponding FFT of the high resolution image.

Fast Fourier transforms (FFTs) are presented in Figure 5. The sample irradiated with 300 keV Ar at 7.7×10^{14} ions/cm^2 (0.8 dpa) is considered to be our reference sample to study the initial structural modifications after Ar irradiation. Here, it is assumed that the 0.7 and 0.8 dpa samples are similar in terms of their structure as seen by RBS/C derived damage versus depth profiles (see Figures 1(a) and 1(b) in Ref. [11]). In Figure 5(a), the 0.8 dpa sample can be marked by the presence of a damaged layer that extends upto a depth of about 300 nm from the sample surface, supporting the RBS/C analysis. Figure 5(b) shows the higher resolution image of the undamaged-damaged interfacial region. The damaged layer consists of disordered/amorphous regions as evidenced by the typical contrast on the high-resolution bright-field images and their corresponding FFTs. In Figure 5(b), the regions marked as 1, 2 and 3 correspond to the region beneath the damaged layer, the interfacial region between the undamaged-damaged layer, and the region within the damaged layer, where maximum damage is expected. As we move from region 1 to region 3, the disappearance of spots in the corresponding FFTs indicates degradation of crystallinity within the damaged layer. The TEM image with excellent resolution and the corresponding FFT from region 2, reveals that the undamaged-damaged interface consists of partially disordered regions (regions having darker contrast) surrounded by crystalline regions. The FFT from region 3 exhibits very low-intensity spots (hardly noticeable) surrounded by diffuse scattering, supporting the conclusion of a heavily damaged region. After annealing, the extension of the damaged layer reduces to 250 nm as shown in Figure 5(c). Further, the HR-TEM image of the damaged layer presented in Figure 5(d), shows that annealing results in a less disordered microstructure, where crystalline areas surround the residual damaged regions. The corresponding FFT of the damaged layer (inset to Figure 5(d)) show multiple aligned spots, indicating an improved crystallinity and absence of heavily disordered/amorphous regions. The TEM analysis reveals that annealing leads to a recovery of the extended disordered regions towards regions having less

disordered microstructure. The TEM analysis corroborates the RBS/C and XRD results. Besides, TEM reveals some degree of crystallinity that the HR-XRD data also suggested (as the DW is very low but not completely zero), in contrast to RBS/C which shows the presence of continuous amorphous regions. This is due to the differences in probe-sample interaction of various experimental techniques.

4 Conclusion

Summarizing, we studied the recovery of pre-damaged 4H-SiC single-crystals irradiated using 300 keV Ar ions by performing thermal treatment at various temperatures from 673 K to 1273 K. Rutherford backscattering spectrometry in channeling geometry (RBS/C), Raman scattering and high-resolution X-ray diffraction were used to investigate the microstructural modifications and strain depth profiles in the irradiated and annealed crystals. RBS/C results showed that the sample with an initial damage level of 0.7 dpa (TRIM estimated) has an extended amorphous region that is centred at a ∼175 nm depth and has a width of about 200 nm. Thermal annealing resulted in the shrinkage of this amorphous region and a reduction in the initial disorder across the entire pre-damaged layer (∼300 nm). This result is supported by Raman data that suggests a significant improvement in the chemical ordering upon thermal treatment and the ion irradiation-related features including the disordered Si-C, C-C and Si-Si bands are suppressed. After the final annealing at 1273 K, the first-order Raman mode of 4H-SiC i.e. E_2(TO) dominates the entire spectrum similar to that of the pristine crystal. RBS/C and Raman results estimate a lattice recovery of about 54.4% and 52.1%, respectively. Extensive strain and disorder analyses from the HR-XRD data reveal that increasing Ar ion-irradiation fluence on 4H-SiC leads to a saturation of maximum strain at 12% with a very low DW factor. After the final annealing at 1273 K, the maximum strain reduces from 12% to 2% and this reduction is attributed to the lattice recovery initiated by the movement of $\sim 7 \times 10^{16}$ atoms. In-situ annealing during HR-XRD measurements allowed the determination of the evolution of strain with thermal damage annealing. The TEM analysis, on a qualitative level, illustrates the thermal recovery of the microstructure. It can be concluded that the strain can be engineered with extreme control using ion-irradiation and subsequent annealing at the desired temperature.

Supplementary information

A detailed description of the HR-XRD experimental technique is supplied as a supporting Information.

Acknowledgments

AC acknowledges the Council of Scientific and Industrial Research (CSIR), India for financial support through fellowship. The low energy ion beam facility

and Rutherford backscattering spectrometry groups at IUAC, New Delhi, India are acknowledged for their assistance.

Declarations

Conflict of interest The authors declare that they have no known competing financial interests or personal relationships that could have appeared to influence the work reported in this paper.

References

[1] Atatüre M, Englund D, Vamivakas N, Lee S-Y, Wrachtrup J (2018), Material platforms for spin-based photonic quantum technologies, Nat. Rev. Mater. 3:38

[2] Awschalom D D, Hanson R, Wrachtrup J, Zhou B B (2018), Quantum technologies with optically interfaced solid-state spins, Nat. Photonics, 12:516

[3] Koehl W F, Buckley B B, Heremans F J, Calusine G, Awschalom D D (2011), Room temperature coherent control of defect spin qubits in silicon carbide, Nature, 479:84

[4] Lohrmann A, Johnson B C, McCallum J C, Castelletto S (2017), A review on single photon sources in silicon carbide, Reports on Progress in Physics , 80:034502

[5] Rueb M, A novel ion-implantation technique improves the manufacture of SiC power devices, including super-junction MOSFETs, Compound Semiconductor, Volume 25 Issue 3, April/May 2019. https://publishing.ninja/V4/page/9077/377/6/

[6] Debelle A, Thomé L, Dompoint D, Boulle A, Garrido F, Jagielski J, Chaussende D (2010), Characterization and modelling of the ion-irradiation induced disorder in 6H-SiC and 3C-SiC single crystals, J. Phys. D: Appl. Phys. 43:455408

[7] Debelle A, Boulle A, Chartier A, Gao F, Weber W J (2014), Interplay between atomic disorder, lattice swelling, and defect energy in ion-irradiation-induced amorphization of SiC, Phys. Rev. B 90:174112

[8] Boulle A, Debelle A, Wallace J B, Bayu Aji L B, Kucheyev S O (2017), The amorphization of 3C-SiC irradiated at moderately elevated temperatures as revealed by X-ray diffraction, Acta Materialia 140:250

[9] Zhang F X, Tong Y, Xue H, Keum J K, Zhang Y, Boulle A, Debelle A, Weber W J (2019), Strain engineering 4H-SiC with ion beams, Appl. Phys.

Lett. 114:221904

[10] Chakravorty A, Singh B, Jatav H, Ojha S, Singh J, Kanjilal D, Kabiraj D (2020), J. Appl. Phys. 128:165901

[11] Chakravorty A, Ch Dufour Ch, Singh B, Jatav H, Umapathy G R, Kanjilal D, Kabiraj D (2021), Recovery of ion-damaged 4H-SiC under thermal and ion beam-induced ultrafast thermal spike-assisted annealing, J. Appl. Phys. 130:165901

[12] Chakravorty A, Singh B, Jatav H, Meena R, Kanjilal D, Kabiraj D (2021), Controlled generation of photoemissive defects in 4H-SiC using swift heavy ion irradiation, J. Appl. Phys. 129:245905

[13] Chakravorty A, Jatav H, Singh B, Ojha S, Kabiraj D (2021), 300 keV Ar ion induced effects in GaAs and 4H-SiC, in Proceedings of the National Conference on Recent Advances in Functional Materials (RAFM-2020), Materials Today: Proceedings 47:1633

[14] Kalikka J, Zhou X, Dilcher E, Wall S, Li J, Simpson R E (2016), Strain-engineered diffusive atomic switching in two-dimensional crystals, Nat. Commun. 7:11983

[15] Leclerc S, Declemy A, Beaufort M F, Tromas C, Barbot J F (2005), Swelling of SiC under helium implantation, J. Appl. Phys. 98:113506

[16] Leclerc S, Beaufort M F, Declemy A, Barbot J F (2006) Damage induced in high energy helium-implanted 4H-SiC, Nucl. Instrum. Methods Phys. Res. 242:399

[17] Sorieul S, Costantini J-M, Gosmain L, Thome L, Grob J-J (2006), Raman spectroscopy study of heavy-ion-irradiated α-SiC, J. Phys.: Condens. Matter 18:5235

[18] Benyagoub A, Audren A, Thome L, Garrido F (2006), Athermal crystallization induced by electronic excitations in ion-irradiated silicon carbide Appl. Phys. Lett. 89:241914

[19] Declemy A, Debelle A, Dupeyrat C, Thome L, Monnet I, Eyidi D(2012), Correlation between implantation defects and dopants in Fe-implanted SiC, Appl. Phys. A: Mater. Sci. Process. 106:679

[20] Gärtner K (2005), Modified master equation approach of axial dechanneling in perfect compound crystals, Nucl. Instrum. Methods Phys. Res. Sect. B , 227, 522,

[21] Weber W J, Zhang Y (2019), Predicting damage production in monoatomic and multi-elemental targets using stopping and range of ions in matter code: Challenges and recommendations, Curr. Opin. Solid State Mater. Sci. , 23:100757

[22] Ziegler J F, Ziegler M D, Biersack J P, SRIM - The stopping and range of ions in matter (2010), Nucl. Instrum. Method Phys. Res. B 2010, 268:1818

[23] Devanathan R, Weber W J, Gao F (2001), Atomic scale simulation of defect production in irradiated 3C-SiC, J. Appl. Phys. , 90:2303–2309

[24] Souilah M, Boulle A, Debelle A (2016), RaDMaX: a graphical program for the determination of strain and damage profiles in irradiated crystals, J. Appl. Cryst. 49:311

[25] Boulle A, Mergnac V (2020), RaDMaX online: a web-based program for the determination of strain and damage profiles in irradiated crystals using X-ray diffraction, J. Appl. Cryst. 53:587

[26] Takagi S(1969), A Dynamical Theory of Diffraction for a Distorted Crystal, J. Phys. Soc. Jpn. 26:1239

[27] Taupin D (1964), Théorie dynamique de la diffraction des rayons X par les cristaux déformés, Bull Soc Fr. Minér Crist. 87:469

[28] Bartels W J, Hornstra J, Lobeek D J K (1986), X-ray diffraction of multilayers and superlattices, Acta Cryst. 42:539

[29] Benyagoub A, Audren A (2009), Mechanism of the swift heavy ion induced epitaxial recrystallization in predamaged silicon carbide, J. Appl. Phys. 106:083516

[30] Debelle A, Backman M, Thomé L, Weber W J, Toulemonde M, Mylonas S, Boulle A, Pakarinen O H, Juslin N, Djurabekova F, Nordlund K, Garrido F, Chaussende D (2012), Material Transformation: Interaction between Nuclear and Electronic Energy Losses, Phys. Rev. B 86:100102(R)

[31] Debelle A, Thomé L, Monnet I, Garrido F, Pakarinen O H, Weber W J (2019), Ionization-induced thermally activated defect-annealing process in SiC, Phys. Rev. Mater. 3:063609

[32] Burton J C, Sun L, Pophristic M, Lukacs S J, Long F H, Feng Z C, Ferguson I T (1998), Spatial characterization of doped SiC wafers by Raman spectroscopy, J. Appl. Phys. 84:6268

[33] Burton J C, Sun L, Long F H, Feng Z C, Ferguson I T (1999), First- and second-order Raman scattering from semi-insulating 4H-SiC, Phys. Rev.

B, 59:7282

[34] Nakashima S, Harima H (1997), Raman Investigation of SiC Polytypes, Phys. Status Solidi A, 162:39

[35] Nakashima S, Kitamura T, Mitani T, Okumura H, Katsuno M, Ohtani N (2007), Raman scattering study of carrier-transport and phonon properties of 4H-SiC crystals with graded doping, Phys. Rev. B, 76:245208

[36] Sorieul S, Kerbiriou X, Costantini J-M, Gosmain L, Calas G, Trautmann C (2012), Optical spectroscopy study of damage induced in 4H-SiC by swift heavy ion irradiation, J. Phys. Condens. Matter 24:125801

[37] Lannin L S, Pilione L J, Kshirsagar S T, Messier R, Ross R C (1982), Variable structural order in amorphous silicon, Phys. Rev. B 26:3506(R)

[38] Zwick A, Carles R, Multiple-order Raman scattering in crystalline and amorphous silicon (1993), Phys. Rev. B 48:6024

[39] Ehbrecht M, Ferkel H, Huisken F, Holz L, Polivanov Y N, Smirnov V V, Stelmakh O M, Schmidt R (1995), Deposition and analysis of silicon clusters generated by laser-induced gas phase reaction., J. Appl. Phys. 78:5302–5306

[40] Usman M, Nour M, Azarov A Y, Hallén A (2010), Annealing of ion implanted 4H–SiC in the temperature range of 100–800 °C analysed by ion beam techniques, Nucl. Instrum. Methods Phys. Res. B 268:2083

[41] Boulle A, Debelle A (2010), Strain-profile determination in ion-implanted single crystals using generalized simulated annealing, J. Appl. Cryst. 43:1046

[42] Leclerc S, Beaufort M F, Barbot J F, Declémy A (2012), Strain and amorphization under light-ion implantation in SiC, EPL 98:46001

[43] Pietsch U, Holy V, Baumbach T, High-resolution X-ray Scattering from Thin Films to Lateral Nanostructures, Springer-Verlag, New York, 2004. LLC.

[44] Boulle A, Debelle A (2016), Statistical Nature of Atomic Disorder in Irradiated Crystals, Phys. Rev. Lett. 116:245501

[45] Jiang W, Zhang Y, Weber W J (2004), Temperature dependence of disorder accumulation and amorphization in Au-ion-irradiated 6H-SiC, Phys. Rev. B 70:165208

[46] Zheng M J, Swaminathan N, Morgan D, Szlufarska I (2013), Energy barriers for point-defect reactions in 3C-SiC, Phys. Rev. B 88:054105

[47] Coutinho J (2021), Theory of the Thermal Stability of Silicon Vacancies and Interstitials in 4H–SiC, Crystals, 11(2):167

[48] Wang J F, Li Q, Yan F F, Liu H, Guo G P, Zhang W P, Zhou X, Guo L P, Lin Z H, Cui J M, Xu X Y, Xu J S, Li C F, Guo G C (2019), On-Demand Generation of Single Silicon Vacancy Defects in Silicon Carbide, ACS Photonics 6:1736

[49] Chakravorty A, Kabiraj D (2022), Luminescence from color centres induced by oxidation and ion irradiation in 4H–SiC, J. Lumin. 244:118713

[50] Rühl M, Ott C, Götzinger S, Krieger M, Weber H B (2018), Controlled generation of intrinsic near-infrared color centers in 4H-SiC via proton irradiation and annealing, Appl. Phys. Lett. 113:122102